THE JOURNAL OF PHYSICAL CHEMISTRY B

Article

pubs.acs.org/JPCB

3D Structures and Redox Potentials of Cu^{2+}–Aβ(1–16) Complexes at Different pH: A Computational Study

Jorge Alí-Torres, Andrea Mirats, Jean-Didier Maréchal, Luis Rodríguez-Santiago, and Mariona Sodupe*

Departament de Química, Universitat Autònoma de Barcelona, 08193 Bellaterra, Barcelona, Spain

Supporting Information

ABSTRACT: Oxidative stress induced by redox-active metal cations such as Cu^{2+} is a key event in the development of Alzheimer's disease. A detailed knowledge of the structure of Cu^{2+}–Aβ complex is thus important to get a better understanding of this critical process. In the present study, we use a computational approach that combines homology modeling with quantum-mechanics-based methods to determine plausible 3D structures of Cu^{2+}–Aβ(1–16) complexes that enclose the different metal coordination spheres proposed experimentally at different pH values. With these models in hand, we determine their standard reduction potential (SRP) with the aim of getting new insights into the relation between the structure of these complexes and their redox behavior. Results show that in all cases copper reduction induces $CO_{backbone}$ decoordination, which, for distorted square planar structures in the oxidized state (Ia_$\delta\delta$, IIa_$\varepsilon\delta\varepsilon$, IIa_$\varepsilon\varepsilon\varepsilon$, and IIc_$\varepsilon$), leads to tricoordinated species. For the pentacoordinated structural candidate Ib_$\delta\varepsilon$ with Glu11 at the apical position, the reduction leads to a distorted tetrahedral structure. The present results highlight the importance of the nature of the ligands on the SRP. The computed values (with respect to the standard hydrogen electrode) for complexes enclosing negatively charged ligands in the coordination sphere (from −0.81 to −0.12 V) are significantly lower than those computed for models involving neutral ligands (from 0.19 to 0.28 V). Major geometry changes induced by reduction, on both the metal site and the peptide configuration, are discussed as well as their possible influence in the formation of reactive oxygen species.

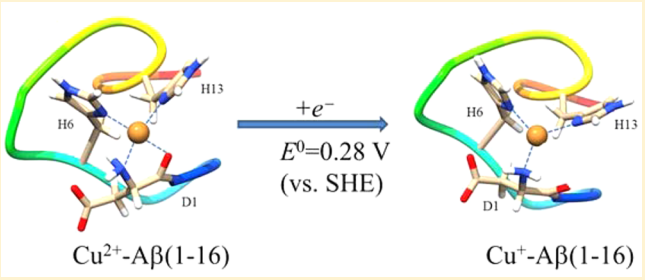

I. INTRODUCTION

Alzheimer's disease (AD) is the most common form of neurodegenerative dementia, affecting ∼45% of people over 85 years.[1] It is characterized by structural changes in the brain that generate a progressive loss on neuronal abilities, and its most important hallmarks are the formations of neurofibrillary tangles and extracellular senile plaques.[2,3] These plaques are formed mainly by the deposition of the β-amyloid peptide (Aβ), a small peptide between 39 and 42 amino acids long,[2] obtained from the abnormal cleavage of amyloid precursor protein (APP). Metal–Aβ complexes enclosing redox-active metal cations such as Cu^{2+} or Fe^{3+} have been shown to be involved in the increase in oxidative stress.[4,5] This oxidative damage, which precedes Aβ deposition,[6,7] can cause oxidation of proteins and DNA[4] and increase lipid peroxidation, as these processes are the most fatal features observed in the development of the AD.[8] It is postulated that metal–Aβ complexes participate in these processes by leading to the formation of reactive oxygen species (ROS).[9,10] In particular, they are hypothesized to contribute to the production of H_2O_2, which, in turn, derives in the production of ROS through Fenton and Haber–Weiss-like reactions.[11−16]

In the case of copper, the first step in the production of ROS species is the reduction of the metal cation in the Cu^{2+}–Aβ complex. The first studies reported values of 0.72 to 0.77 V versus standard hydrogen electrode (SHE) for the standard reduction potential (SRP) of the Cu^{2+}–Aβ/Cu^{+}–Aβ couple.[9] These values have been later on considered too high, the more recent values ranging from 0.28 to 0.34 V.[14,16,17] Initially, this reduction was proposed to be induced by the Aβ itself,[18] through the oxidation of some residues such as Tyr10 and Met35. However, Tyr10 and Met35 were discarded due to their high redox potentials (0.95 and 1.5 V, respectively),[14,19] as compared with that reported for the Cu^{2+}–Aβ/Cu^{+}–Aβ couple. Moreover, similar values were found for Cu^{2+}–Aβ(1–16), Cu^{2+}–Aβ(1–28), and Cu^{2+}–Aβ(1–42) complexes, thereby excluding that Met35 acts as the reducing agent in the process[14] and suggesting that the mechanism for ROS production probably involves some of the external reducing agents usually present in the cerebral medium.

The reduced Cu^{+}–Aβ complex reacts with the dissolved oxygen and the protons in the medium to give the Cu^{2+}–Aβ-oxidized system, which could be further reduced, resulting in a catalytic cycle that would generate hydrogen peroxide in excess (Figure 1). The global reaction is as follows:

Received: February 25, 2014
Revised: April 11, 2014
Published: April 16, 2014

   dx.doi.org/10.1021/jp5019718 | J. Phys. Chem. B 2014, 118, 4840–4850

$$2Cu^{+} - A\beta + O_2 + 2H^{+} \rightarrow 2Cu^{2+} - A\beta + H_2O_2$$

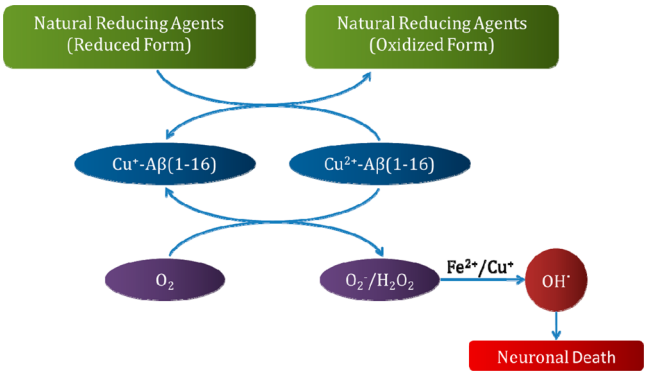

Figure 1. Schematic representation of the catalytic cycle responsible of the generation of ROS.

The SRP versus SHE for the couple O_2/H_2O_2 is 0.30 V at physiological pH.[20] In this vein, the production of H_2O_2 is thermodynamically favored if: (i) the SRP for the copper complex is higher than those of the external reducing agents and (ii) it is lower than that for the O_2/H_2O_2 couple. Azimi and Rauk[21] have computationally determined the SRP for several cluster models of copper−Aβ complexes, enclosing different coordination spheres, and obtained values that range from −0.07 to 0.63 V, which highlights the relevance of the coordination mode on the redox properties of the complex. Similarly, the study by Liu et al. on copper-prion protein (PrP) complexes has shown that the redox cycling of Cu^{2+} critically depends on the binding mode of the PrP−Cu^{2+} complex.[22]

In the past decade many conflicting spectroscopic studies on the Cu^{2+}−Aβ coordination have been published.[23−35] Excellent reviews discussing the ensemble of putative Cu^{2+} coordination spheres have recently appeared.[36−38] The latest studies by means of continuous-wave electron paramagnetic resonance (CW-EPR) spectroscopy and hyperfine sublevel correlation (HYSCORE) provide support for a 3N1O coordination sphere in Cu^{2+}−Aβ(1−16)[26,27,34,35] and reveal the existence of two main species in the physiological pH range: one referred to component I at low pH (<7) and a second one, named component II, at higher pH. (See Scheme 1.) At pH 6.3 to 6.9, the Cu^{2+} coordination sphere involves the binding of the terminal amino group, His6 and His13 (or His14), and an oxygen atom from Asp1,[26,27,35] whereas at pH 8 coordination is due to the three histidine residues and the carbonyl group of Ala2.[26] At higher pH (8.7), only one His along with the NH_2 terminus, the deprotonated amide nitrogen of Ala2, and a carbonyl oxygen are equatorial ligands of Cu^{2+}.[34] From a computational perspective, several studies have addressed the coordination of Cu^{2+} interacting with Aβ.[12,21,39−45] Quantum chemical calculations have mostly been applied to small model systems,[12,39,43] including the first coordination sphere of the metal cation, whereas larger systems including the whole Aβ have been considered through classical molecular dynamic simulations.[24,40,41] Electronic structure calculations for intermediate size models such as Cu^{2+}−Aβ(1−7)[45] or Cu^{2+}−Aβ(1−16)[44,46] have also recently been described. However, to our knowledge, structures for all Cu^{2+}−Aβ(1−16) complexes, enclosing the different experimentally proposed coordination environments, (components Ia/Ib, IIa, and IIc) have not yet been reported.

The present work has two main goals. The first one is to provide 3D structures for Cu^{2+}−Aβ(1−16) complexes enclosing the different coordination spheres proposed experimentally at different pH. This is done computationally by combining homology modeling (HM) techniques with quantum-mechanics (QM)-based approaches, following the protocol used in our previous study,[44] but improving the model refinement step by performing full DFT instead of DFT/MM optimizations as well as including implicitly the influence of the solvent. (See the Computational Methods.) The second one is to determine the SRP of these complexes because different coordination modes in Cu^{2+}−Aβ are expected to present different redox properties. Major geometry changes induced by reduction, on both the metal site and the peptide conformation, will be discussed as well as their possible influence in the formation of ROS.

II. COMPUTATIONAL METHODS

The protocol used for the construction of the Cu^{2+}−Aβ(1−16) models is shown in Figure 2. The protocol starts by studying restricted models that include the first coordination sphere of the metal with QM techniques. The geometry of each putative configuration is optimized with density functional theory (DFT) methods. Subsequently, an initial model of the entire metal−Aβ complex is generated using HM approaches. In this part of the protocol, the geometrical variables related to the first coordination sphere of the metal are included in the calculation as additional special constraints. Many candidates are generated in HM runs for each metal configuration, and a series of structural filters is used to select those that are the most probable ones. The models are finally refined with quantum chemical calculations. By allying QM and HM in a unique workflow, we make the hypothesis that all minima of divalent cations bounds to Aβ are not far one from the other on the potential energy surface. As a consequence, we can use a unique

Scheme 1. Coordination Spheres Proposed Experimentally for the Different Cu^{2+}−Aβ(1-16) Complexes from CW-EPR Spectroscopy[36]

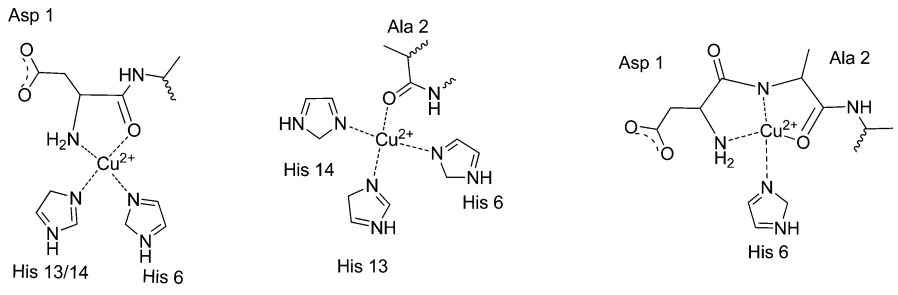

dx.doi.org/10.1021/jp5019718 | J. Phys. Chem. B 2014, 118, 4840−4850

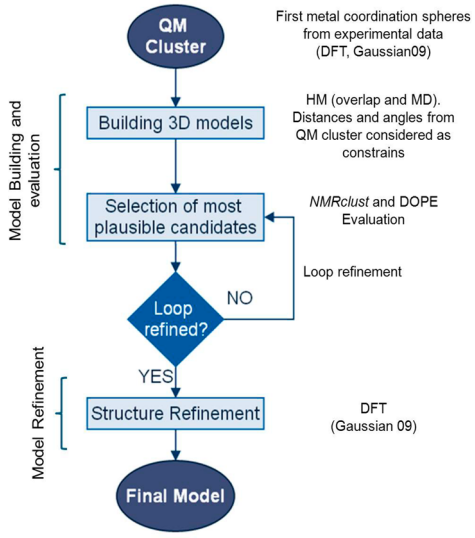

Figure 2. Protocol used for the construction and evaluation of the Cu^{2+}-Aβ(1−16) models.

structure as a starting point of the HM step (in our case the Zn^{2+}−Aβ one, PDB code 1ZE9),[47] alter the first coordination sphere to satisfy copper geometries, and optimize all the peptidic environment. This multiscale protocol shares common grounds with the one reported in our previous study on the component IIa Cu^{2+}−Aβ.[44] However, the present procedure has been improved with systematic minimizations at a full QM level and including solvent effects of all possible Cu^{2+}−Aβ structural candidates and finer optimizations of the conformation of their loops. (See Figure 2.)

Homology Modeling Simulations. HM calculations were carried out by using the conformation of Aβ in the Zn^{2+}−Aβ(1−16) complex reported in the Protein Data Bank (PDB code, 1ZE9)[47] as template and including geometry restraints (distances and angles) derived from DFT calculations on small copper complexes representing the metal binding site. These HM calculations were carried out with the Modeler 9v11 package.[48] Both δ and ε coordination of all histidines (6, 13, and 14) and their combinations were evaluated. For each type of coordination, 500 homology models were generated. The models for each configuration were grouped using the Ensemble Cluster protocol implemented in Chimera 1.7,[49] and the most representative model for each cluster was selected. These models were evaluated energetically and geometrically using the Discrete Optimized Protein Energy (DOPE) method implemented in Modeler 9v11[50] to determine the best candidate for each coordination. Starting from the best candidate, additional simulations with finer refinement of the flexible amyloid loop were carried out to generate 100 new HM models that were again evaluated following the same previously mentioned protocol. Overall, the wide range of RMSD values obtained for our final models suggests that we have sampled a large conformational space and thus that these simulations should be able to catch physically plausible models of Cu^{2+}−Aβ(1−16). However, these models do not include the electronic structure effects on the metal binding site of the whole system. Therefore, these candidates were thereafter fully optimized with DFT, as described in the next subsection.

Electronic Structure Methods. The functional chosen for this work needs to properly describe the coordination properties of the metal site as well as the peptide configuration. With respect to the metal site, previous studies for Cu^{2+}−L systems have shown that GGA functionals or hybrid functionals with a low percentage of exact exchange tend to overstabilize lower coordinated structures due to spin delocalization.[51,52] Indeed, for $Cu^{2+}(H_2O)_n$ clusters, the BLYP and hybrid B3LYP functionals were found to clearly favor four-coordinated structures over five-coordinated ones, whereas functionals with higher percentage of exact exchange such as MPWB1K and BHLYP (44 and 50% of exact exchange, respectively) provided quasi-degenerate structures for both coordinations (relative energies lie between 0.2 and 2.4 kcal mol^{-1} depending on the functional and system), in agreement with CCSD(T) results.[51] In the present work, calculations have been carried out with the more recently developed meta-hybrid M06-2X functional,[53] which encloses 54% of exact exchange. With this functional, calculations for the $Cu^{2+}(H_2O)_6$ system with five and four water molecules in the first coordination sphere indicate that fourth and fifth coordinations are quasi-degenerate (relative stability is −0.5 kcal mol^{-1}), as found previously with CCSD(T). Moreover, this functional provides a second ionization energy of Cu (20.2 to 20.6 eV depending on whether we use an all-electron basis set or an effective core potential), in good agreement with the experimental value (20.3 eV),[54] which is an important issue for the computation of Cu^{2+}−Aβ/Cu^{+}−Aβ redox potentials. Finally, M06-2X accounts for dispersion forces, which are important to properly account for the peptide configuration and stability.[53] Nevertheless, and because M06 has been more recommended for transition-metal systems than M06-2X, we have performed calculations for the metal site with M06, M06L, and M06-2X functionals. Results, given in Figure S1 of the Supporting Information, show that there are minor structural differences.

M06-2X full geometry optimizations and frequency calculations were done using the LANL2DZ pseudopotential and its associated basis set for copper (5s5p5d)/[3s3p2d][55] and the standard 6-31G(d) basis set for the rest of atoms. Final energies were, however, refined by performing single-point calculations with the larger LANL2TZ (5s5p5d)/[5s5p3d] basis set for Cu[56] supplemented with an f function[57] and the 6-311++G(d,p) for the remaining atoms. Hereafter, the two basis sets used will be referred to as small basis (SB) and large basis (LB), respectively. This is a cost-efficient strategy because both basis sets provide very similar geometrical parameters. (See Figures S1 and S2 in the SI.) Full optimizations and frequency calculations were done considering solvent (aqueous) effects using the SMD implicit solvation model,[58] and thus residues were considered in the protonation states expected in solution at physiological pH. Starting structures in these optimizations were taken from HM simulations and, to save computer time, they were first relaxed with ONIOM (M06-2X:UFF) in the gas phase, with the first coordination sphere in the high-level region and residues considered in their neutral form. It is worth noting that the peptide backbone after full DFT optimization shows only minor modifications compared with the HM initial models.

Thermodynamic corrections were obtained assuming unscaled harmonic vibrational frequencies, and the rigid rotor approximation was obtained by standard statistical methods. We confirmed all structures as true minima by calculating the vibrational frequencies. However, it should be noticed that in few cases the optimized structure showed low imaginary frequencies (<50 cm^{-1} in absolute value). Because of the size of the system and thus of the computational cost, reoptimizations

dx.doi.org/10.1021/jp5019718 | J. Phys. Chem. B 2014, 118, 4840−4850

Table 1. Relative Energies for Components Ia and Ib[a]

models	ΔE	ΔE_{MC}	ΔE_{pept}	ΔH	$T\Delta S$	ΔG	N_{HB}	N_{SB}	SB_{HB}
				Ia = [CO^{D1}, N_{ter}, N^{H6}, N^{H13}]					
Ia_$\delta\delta$	0.0	0.0	0.0	0.0	0.0	0.0	10	$2_{(E3\text{-}K16/R5\text{-}D7)}$	1.64/1.91, 1.98
Ia_$\delta\varepsilon$	19.1	−4.1	21.8	18.3	13.7	4.6	5	$1_{(R5\text{-}D7)}$	1.80
Ia_$\varepsilon\delta$	23.8	0.2	26.7	23.8	9.8	13.9	6	$1_{(K16\text{-}CO2\text{-}ter)}$	1.69
Ia_$\varepsilon\varepsilon$	18.4	−6.6	22.5	18.4	8.0	10.4	7	$1_{(D1\text{-}R5)}$	1.91, 189
				Ib = [CO^{D1}, N_{ter}, N^{H6}, N^{H14}]					
Ib_$\delta\delta$	35.0	−4.3	37.8	34.5	18.0	16.5	5	0	
Ib_$\delta\varepsilon$	16.0	−2.1	30.0	15.7	13.1	2.6	5	0	
Ib_$\varepsilon\delta$	14.1	−5.6	24.3	13.2	7.6	5.6	4	$1_{(E3\text{-}K16)}$	1.61
Ib_$\varepsilon\varepsilon$	21.9	−3.5	28.7	20.3	12.8	7.5	8	$1_{(E3\text{-}K16)}$	1.86

[a] ΔE_{MC} and ΔE_{pept} are the relative energies of the metal center and the peptide moiety, respectively. N_{HBC} is the total number of hydrogen bond contacts (hydrogen bond cutoff distance ≤2.1 Å) observed in the peptidic moiety, and N_{SB} is the number of salt bridges. All energies are in kilocalories per mole. Distances in angstroms.

to find the true minima were not carried out. Instead, and because the imaginary frequencies were all quite small, their contribution to the molar enthalpy was considered to be RT, as for a low-frequency vibration, and their contribution to the entropy was estimated considering a frequency of 10 cm^{-1} for each imaginary one, as done previously.[59]

Open-shell calculations were based on an unrestricted formalism. All electronic structure calculations have been performed with the Gaussian 09 set of programs.[60] Atomic charges and spin densities were obtained from natural population analysis (NPA).

Standard Reduction Potential Calculations. The most stable models obtained for the Cu^{2+}−Aβ(1−16) complexes were reduced and reoptimized to obtain the corresponding Cu^{+}−Aβ(1−16) ones. Additionally, frequency calculations were performed to estimate the thermochemical properties. Thus, the SRP versus the SHE was estimated considering the following semi-reactions

$$\text{`}Cu^{2+}\text{'}_{(aq)} + e^- \rightarrow \text{`}Cu^{+}\text{'}_{(aq)} \qquad \Delta G^{Cu}$$

and

$$H^+ + e^- \rightarrow 1/2H_2 \qquad \Delta G^{SHE}$$

where 'Cu^{2+}' and 'Cu^{+}' represent the oxidized and reduced species of the $Cu^{2+/+}$−Aβ(1−16) couple in aqueous solution, respectively, and ΔG^{Cu} and ΔG^{SHE} are the free-energy changes for the semi-reactions, ignoring the electron. Thus, the SRP is calculated using the following equation

$$E^{\circ}(\text{`}Cu^{2+}\text{'}/\text{`}Cu^{+}\text{'}) = -\Delta G^{0}_{Cu} - \Delta G^{0}_{SHE}/F$$

where F is the Faraday constant (23.061 kcal V^{-1} mol^{-1}). For the reduction of the proton in aqueous solution, we used the experimental value, ΔG^{SHE} = −99.9 kcal mol^{-1}.[12,61] To account for the limitations on the level of theory used, an empirical correction, defined as the difference between the calculated and experimental SRP for the $[Cu^{2+}(H_2O)_4]^{+}/[Cu^{+}(H_2O)_4]^{2+}$ couple, was added to the SRP calculations.

III. RESULTS AND DISCUSSION

This section is organized as follows. First, we will present and discuss the salient features of the 3D structures of Cu^{2+}−Aβ(1−16) complexes with the proposed experimental coordination environments. (See Scheme 1.) Second, we will discuss their redox properties and their possible influence in the formation of ROS species.

Three-Dimensional Structures of Cu^{2+}-Aβ(1−16). *Cu^{2+}−Aβ(1−16) Complexes at Low pH.* As previously mentioned, low pH component is found at pH values between 6 and 7. Several studies agree that the coordination environment for this component involves the coordination of the N terminus, the CO group from the Asp1 backbone, and two histidines (His6 and His13 for component Ia, and His6 and His14 for component Ib).[27,35] Both δ and ε coordination of the two histidine residues have been considered when constructing the different models, which led to four possible configurations for each group ($\delta\delta$, $\delta\varepsilon$, $\varepsilon\delta$, $\varepsilon\varepsilon$, where the first letter refers to His6 and the second one refers to His13/His14). The relative energies for these models are detailed in Table 1. This Table also includes the relative contributions of the metallic (ΔE_{MC}) and peptidic (ΔE_{pept}) moieties. The ΔE_{MC} values are obtained from single-point calculations of the metal site ($Cu^{2+}(Im)_2(NH_2CH_2CONH_2)$), at the optimized geometry of the Cu^{2+}−Aβ(1−16) complex, whereas ΔE_{pept} results are derived from single-point calculations of the remaining peptidic moiety. In addition, Table 1 includes the total number of hydrogen bond contacts (hydrogen-bond cutoff distance ≤2.1 Å) observed in the peptidic moiety (N_{HB}) and the number of salt bridges (N_{SB}). Optimized geometries for the most stable models for each component are given in Figure 3. Structures for the remaining models are provided in the Supporting Information (Figures S2 and S3). First, it should be noted that all complexes, except Ib_$\delta\varepsilon$, show a distorted square planar coordination environment for the metal site and a spin density of 0.7 to 0.8 at Cu^{2+}. For Ib_$\delta\varepsilon$, an additional interaction with Glu11 lateral chain leads to a square-based pyramid pentacoordination of the metal site, where the spin density is 0.77.

Among all four models of component Ia, the one corresponding to the coordination of the δ nitrogen of both histidines (component Ia_$\delta\delta$) is the most stable. ΔE_{MC} and ΔE_{pept} values indicate that this is due to the higher stabilization of the peptidic moiety because Ia_$\delta\delta$ does not exhibit the most stable coordination environment. Values of ΔE_{MC} indicate that relative energies related to the metal site coordination are minor (~6 kcal mol^{-1}) compared with the peptidic moiety. A detailed analysis of the different structures revealed that the peptide configuration that shows a larger number of hydrogen bond interactions (N_{HBC}) is Ia_$\delta\delta$. Moreover, this model exhibits two salt bridges, one between Glu3 and Lys16 and the other between Arg5 and Asp7, largely contributing to the stability of the complex. As expected, thermal corrections lead

dx.doi.org/10.1021/jp5019718 | J. Phys. Chem. B 2014, 118, 4840−4850

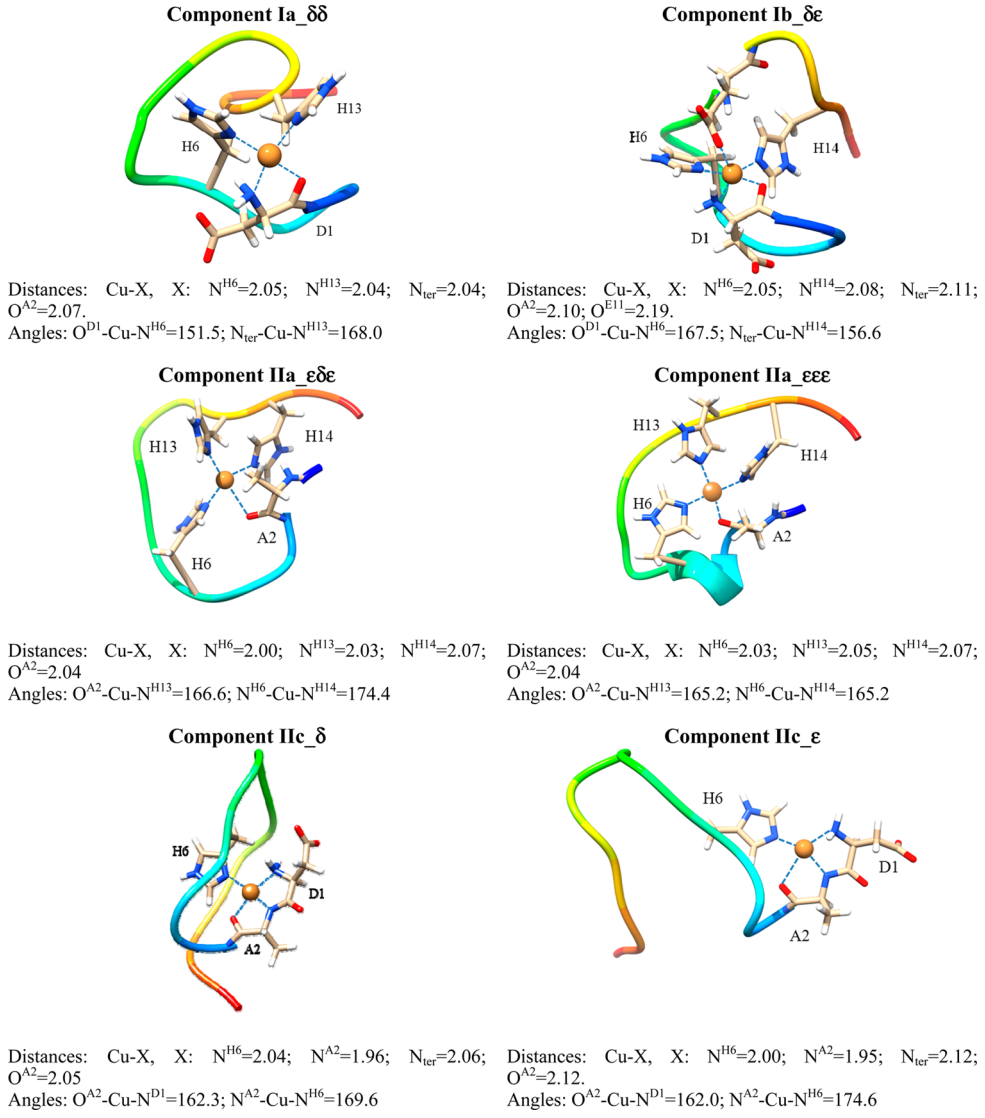

Figure 3. Most stable models for the components considered for Cu^{2+}-Aβ(1−16). Distances are in angstroms and angles in degrees.

Table 2. Relative Energies for Components IIa and IIc[a]

models	ΔE	ΔE_{MC}	ΔE_{pept}	ΔH	$T\Delta S$	ΔG	N_{HB}	N_{SB}	SB_{HB}
IIa = [CO^{A2}, N^{H6}, N^{H13}, N^{H14}]									
IIa_$\delta\delta\delta$	21.0	5.1	16.0	21.8	21.8	4.2	3	0	
IIa_$\delta\delta\varepsilon$	10.6	−1.7	10.4	8.5	6.8	1.7	5	$2_{(K16\text{-}E3/Nter\text{-}D1)}$	1.77/1.60
IIa_$\delta\varepsilon\delta$	30.4	0.7	23.3	32.4	−0.7	33.1	4	0	
IIa_$\delta\varepsilon\varepsilon$	11.4	1.6	12.6	12.3	0.4	11.8	9	$2_{(Nter\text{-}D1/R5\text{-}D1)}$	1.68/2.07
IIa_$\varepsilon\delta\delta$	19.3	−2.9	24.1	20.3	−1.8	22.1	7	$1_{(Nter\text{-}CO2ter)}$	1.70
IIa_$\varepsilon\delta\varepsilon$	7.3	−4.8	10.2	7.2	7.9	−0.7	6	$2_{(Nter\text{-}CO2ter/K16\text{-}D1)}$	1.61/1.79
IIa_$\varepsilon\varepsilon\delta$	35.3	7.9	27.7	34.9	8.2	26.7	9	$2_{(K16\text{-}CO2ter/Nter\text{-}D1)}$	1.85/1.67
IIa_$\varepsilon\varepsilon\varepsilon$	0.0	0.0	0.0	0.0	0.0	0.0	10	$3_{(K16\text{-}D1/Nter\text{-}CO2ter/R5\text{-}D1)}$	1.81/1.59/1.84, 1.98
IIc = [CO^{A2}, N^{A2}, N_{ter}, N^{H6}]									
IIc_δ	0.0	0.0	0.0	0.0	0.0	0.0	8	0	
IIc_ε	13.9	−0.7	8.9	10.6	11.5	−0.9	4	0	

[a] ΔE_{MC} and ΔE_{pept} are the relative energies of the metal center and the peptide moiety, respectively. N_{HBC} is the total number of hydrogen bond contacts (hydrogen bond cutoff distance ≤2.1 Å) observed in the peptidic moiety, and N_{SB} is the number of salt bridges. All the energies are in kilocalories per mole.

to smaller relative free energies due to the lower entropy values of those systems containing more stabilizing interactions. In this regard, the final stability results from a balance between the energy gained due to the formation of such stabilizing interactions and the free energy lost associated with the entropic terms.

For component Ib, relative potential energies (ΔE) indicate that these models lie higher in energy than Ia_$\delta\delta$, despite the

dx.doi.org/10.1021/jp5019718 | J. Phys. Chem. B 2014, 118, 4840−4850

fact that their metal site is more stable. This is again explained from the relative stability of the peptide moiety, which exhibits a smaller number of hydrogen bond contacts, particularly salt-bridge interactions. Indeed, it can be observed in Table 1 that the Ia_$\delta\delta$ model, with two salt bridges, is around 14−24 kcal mol^{-1} more stable than complexes with only one (Ia_$\delta\varepsilon$, Ia_$\varepsilon\delta$, Ia_$\varepsilon\varepsilon$, Ib_$\varepsilon\delta$, and Ib_$\varepsilon\varepsilon$) and 35 kcal mol^{-1} more stable than complex Ib_$\delta\delta$, with no salt bridges, which highlights the magnitude of such interactions. Model Ib_$\delta\varepsilon$ is a particular case because despite not presenting any salt-bridge interaction its relative energy with respect to Ia_$\delta\delta$ is only 16 kcal mol^{-1}. This is due to the additional interaction of Glu11 with the metal cation in Ib_$\delta\varepsilon$, which provides extra stabilization to the complex. Inclusion of thermal effects modifies their relative stability in such a way that Ib_$\delta\varepsilon$ becomes the most stable model for component Ib, in terms of Gibbs free energies, and it lies only 2.6 kcal mol^{-1} higher than complex Ia_$\delta\delta$. Interestingly, none of the conformations of the peptide backbones of the models present an organized secondary structure except model Ia_$\delta\varepsilon$ (see Supporting Information), which exhibits an α-helix structure along residues 11 to 14.

Cu^{2+}−Aβ(1−16) Complexes at High pH. At high pH values (between 8 and 9), two metal coordination spheres have been proposed experimentally: (a) component IIa, which encloses the coordination of CO_{Ala2}, His6, His13, and His14,[26] and (b) component IIc involving the coordination of CO_{Ala2}, N terminus, His6, and the deprotonated amide from the peptidic bond between Ala2 and Asp1.[34,62] For IIa, the different combinations of δ/ε coordination of the three histidines lead to eight configurations. For IIc with only one histidine in the coordination sphere, there are only two possible configurations. Relative energies (ΔE, ΔH, and ΔG) of these configurations are given in Table 2 as well as the number of total hydrogen bond contacts and salt-bridge interactions present in the peptide moiety. Optimized geometries and relevant structural parameters for most stable models of components IIa and IIc are given in Figure 3. Structures for all models considered are provided in Figures S4 and S5, respectively, of the Supporting Information.

All models for component IIa exhibit a distorted square planar coordination and spin density mainly localized at the metal center (0.7 to 0.8). While for most complexes the distortion is minor, for models IIa_$\delta\delta\delta$ and IIa_$\varepsilon\varepsilon\delta$, coordination angles indicate that the distortion is significant. Indeed, these models are the ones that show higher ΔE_{MC} values and thus less stable metal sites. As for low pH component, the final stability of the models depends on an energetic balance between the metallic and peptidic stabilities, the latter being mainly determined by the number of hydrogen-bond and salt-bridge interactions. In addition, thermal contributions play a crucial role in determining the relative stabilities of the derived models. Indeed, when no thermal contributions are considered, the coordination of histidines by the Nε atom (IIa_$\varepsilon\varepsilon\varepsilon$) is the most stable configuration. However, inclusion of thermal effects modifies this preference, with IIa_$\varepsilon\delta\varepsilon$ becoming slightly more stable in terms of Gibbs energies by −0.7 kcal mol^{-1}.

For component IIc, the coordination of the metal center is also square-planar, with the higher rigidity of the Asp1−Ala2 fragment hindering significant distortion. Because of the presence of a tricoordinating fragment, the interaction of His6 through δ or ε N has a minor influence on the relative stability of the metal site, with the final stability of the IIc models being determined by the peptide configuration. Entropic contributions are, however, also crucial to determine the final stability (i.e., δ configuration exhibits lower potential energies but higher Gibbs energies).

Relative stabilities between models IIc and IIa can be obtained from the IIa → IIc + 2H$^+$ reaction free energy. Computed values considering the most stable models (IIa_$\varepsilon\delta\varepsilon$ and IIc_ε) are −1.2, −3.9, and −6.6 kcal mol^{-1} at pH 7, 8, and 9, respectively. That is, component IIc becomes increasingly more stable as the pH increases. While this trend was to be expected, these small values do not allow us to conclusively determine which is the most stable binding site for component II (IIa or IIc) in this pH range. The integrative computational approach used in the present work provides us with the exploration of the conformational space and the modeling of the fine electronic effects necessary to generate physically plausible models of the Cu^{2+}−Aβ complexes, but their relative energies are not definitive. The small differences in energy between complexes make audacious the identification of one particular structure as a unique answer. Indeed, dynamical effects could have entropic contributions that could moderate the relative stabilities between the most stable complexes reported in this work.

Reduction of Cu^{2+}−Aβ(1−16) Complexes. Most stable models identified for each coordination sphere were selected to compute the SRP for the Cu^{2+}−Aβ(1−16)/Cu^{+}−Aβ(1−16) couple. Cu^{+}−Aβ(1−16) models were obtained by reducing the corresponding Cu^{2+}−Aβ(1−16) models and reoptimizing them at the same level of theory. Optimized geometries and relevant structural parameters for the reduced complexes are presented in Figure 4. The computed SRP values are given in Table 3 along with the reactions energies (ΔE, ΔH, and ΔG) associated with the reduction process. Energy values at the geometry of the oxidized system (ΔE_{ver}) have also been included to evaluate which coordination environments are more prone to capture one electron.

As mentioned, to account for the limitations of the level of theory used, we have corrected our values taking as reference the reduction potential of copper in water, modeled through the $[Cu^{2+}(H_2O)_4]^{2+}/[Cu^{+}(H_2O)_4]^{+}$ couple. The experimental value for this couple is 0.16 V,[63] whereas the calculated value of the SRP for this system at the present level of theory is 0.06 V. The difference between the calculated and the experimental values (0.10 V) was added as an empirical correction to the computed SRP of the different Cu^{2+}−Aβ(1−16) complexes. For comparison, and to analyze the influence of Aβ peptide on the SRP of the Cu^{2+}/Cu^{+} couple, we have also computed the reduction potentials for model systems that only include the metal site and the first coordination sphere.

As expected, metal cation reduction induces significant changes in the coordination environment. In particular, reduction induces a decrease in the metal coordination number, from tetracoordinated (pentacoordinated in Ib_$\delta\varepsilon$) in the oxidized Cu^{2+}−Aβ(1−16) species to tricoordinated (tetraccordinated in Ib_$\delta\varepsilon$) in the reduced Cu^{+}−Aβ(1−16) ones. It is noteworthy that most of tricoordinated complexes exhibit T-shaped structures. (See Figure 4.) Major geometrical changes are associated with the Cu^{2+}−$CO_{backbone}$ distance, which increases from ∼2.0 to ∼3.0 Å or >3.0 Å in most cases. The sole exception is IIc_ε, for which the Cu^{2+}−O distance only increases to 2.6 Å, due to the formation of a hydrogen-bond interaction with the backbone that hinders a larger distancing from the metal. In addition, the Cu−N bond distances in the

dx.doi.org/10.1021/jp5019718 | J. Phys. Chem. B 2014, 118, 4840−4850

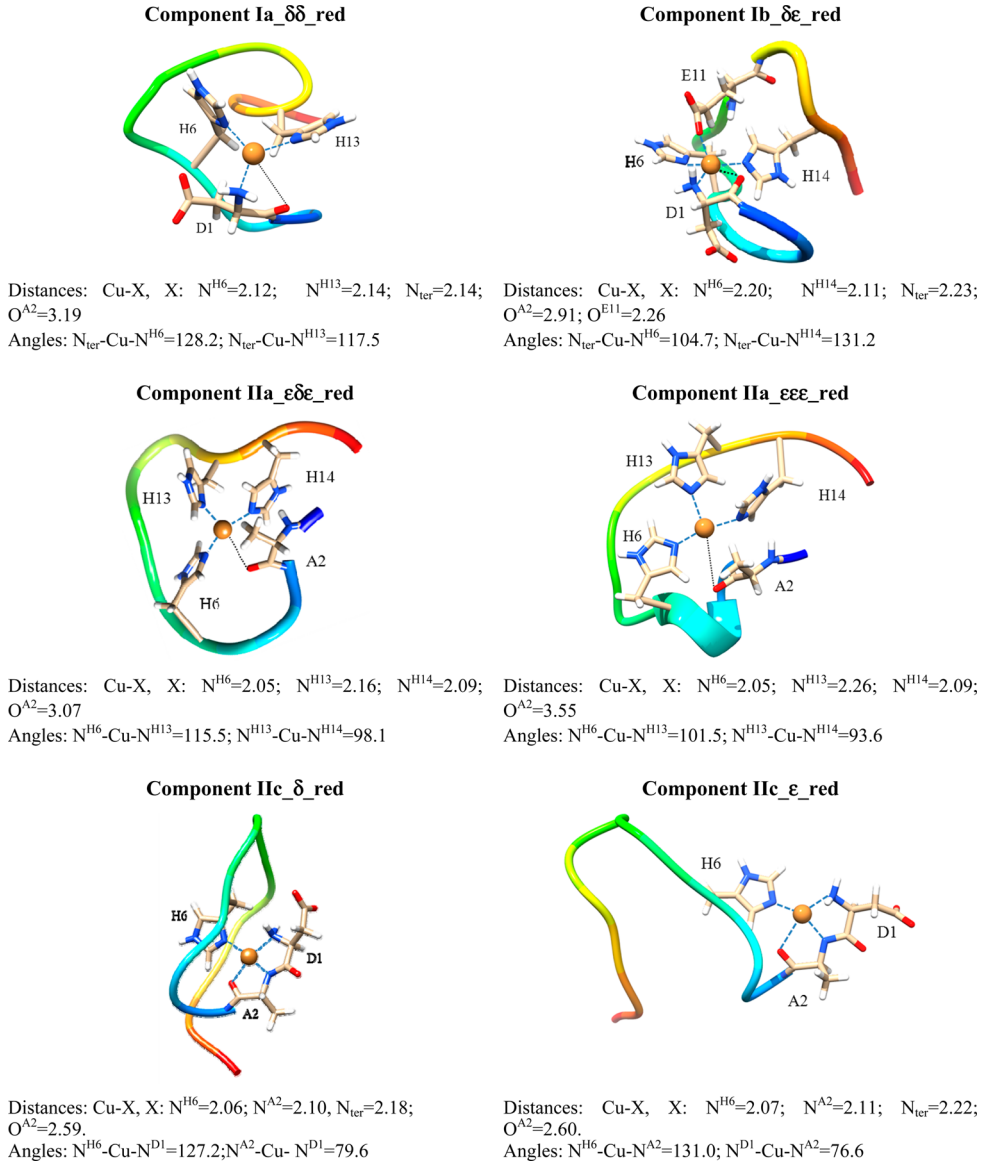

Figure 4. Optimized geometries and relevant geometrical parameters for the reduced Cu^+-Aβ (1−16) models. Distances are in angstroms and angles in degrees.

reduced Cu^+−Aβ(1−16) complexes are larger than those in the oxidized Cu^{2+}-Aβ(1−16) ones due to the smaller electrostatic interaction and larger Pauli repulsion in the formers. This lower metal coordination number for the reduced species is in agreement with X-ray absorption spectroscopy experiments for Cu^+−Aβ model systems, which are consistent with either a two-coordinate linear geometry or three-coordinate T-shaped structures.[64−66] DFT calculations for Cu^+ systems have also demonstrated the propensity of Cu^+ complexes to adopt near-linear two-coordinate or distorted T-shaped structures.[67−69] Although two-coordinate linear species appear to be the most stable, transiently three coordinate ones seem to be more important in the redox cycling[17,64,66,70] because they are more reactive toward dioxygen[64,66] and thus are the species expected to be involved in the reversible redox process. Linear Cu^+ complexes, however, have been found to be inert toward dioxygen.[71]

The peptide conformation exhibits minor changes upon reduction, superimposed models of the oxidized and reduced species showing very similar peptide backbone. (See Figure S6 of the Supporting Information.) Indeed, complex relaxation ($\Delta E - \Delta E_{vert}$), which ranges from −17 to −22 kcal mol^{-1}, is mainly driven by changes on the metal active site. Consistently, relaxation energies in the cluster systems (from −17 to −19 kcal mol^{-1}) are similar to those observed for the peptide complexes. (See Table S1 of the Supporting Information.) Nevertheless, for Ia_$\delta\delta$, IIa_$\varepsilon\delta\varepsilon$, and IIa_$\varepsilon\varepsilon\varepsilon$, the SRP values are larger by 0.12 to 0.32 V as compared with those of the model systems; that is, the reduction of the metal cation seems to be favored in the peptide complex. This arises from several factors such as the distortion induced in the square planar coordination of Cu^{2+}−Aβ by the peptide, the contribution of peptide relaxation, and thermal effects. Note that ∼2.3 kcal mol^{-1} would account for 0.1 V. For models Ib_$\delta\varepsilon$ and IIc_δ, the values of the SRP are very similar to those obtained for the cluster systems. This is due to the higher rigidity of the coordination sphere, which seems to be less influenced by the presence of the peptide. Noteworthy, for IIc_ε, the computed SRP values are smaller than that corresponding to the cluster system. Analysis of the different terms contributing to ΔG

dx.doi.org/10.1021/jp5019718 | J. Phys. Chem. B 2014, 118, 4840−4850

Table 3. Reaction Energies (in kcal mol^{-1}) and Standard Reduction Potential versus Standard Hydrogen Electrode (in volts) for the Most Stable Complexes for the Four Different Components[a]

system	ΔE_{vert}	ΔE	ΔH	$T\Delta S_{298}$	ΔG_{298}	E°_{corr}
$[Cu^{+/2+}(H_2O)_4]^{+/2+}$		−95.7	−98.1	3.1	−101.2	0.16
component Ia_$\delta\delta$	−76.9	−99.1	−100.4	3.7	−104.0	0.28 (−0.04)
component Ib_$\delta\varepsilon$	−74.5	−91.7	−92.9	1.9	−94.8	−0.12(−0.14)
component IIa_$\varepsilon\delta\varepsilon$	−72.5	−96.0	−98.3	4.0	−102.3	0.21 (0.07)
component IIa_$\varepsilon\varepsilon\varepsilon$	−79.7	−99.1	−100.1	1.8	−101.8	0.19 (0.07)
component IIc_δ	−65.9	−87.7	−90.0	−0.9	−89.1	−0.37 (−0.37)
component IIc_ε	−64.7	−85.5	−84.7	−5.8	−78.8	−0.81(−0.37)

[a] ΔE_{vert} is the reduction energy without geometrical changes, while ΔE is the reduction after geometrical relaxation. E°_{corr} is the value estimated considering the empirical correction. (See the text.) Values in parentheses correspond to the model systems at the same level of theory.

indicates that this is due to entropy effects. Note that in IIc_ε discoordination of CO is smaller than that in the model system (the Cu^{2+}−O distance only increases up to 2.6 Å) due to the formation of a hydrogen bond interaction with the backbone (see previous).

Overall, differences on the SRP are mainly due to the changes in the interaction between the copper atom and the ligands present in the first-coordination sphere before and after the reduction process. That is, there is a stronger electrostatic interaction between Cu^{2+} and negative charged ligands (as in components Ib_$\delta\varepsilon$, IIc_δ, and IIc_ε) than between Cu^{+} and the same negatively charged ligand in the reduced models. This loss in the electrostatic interaction upon reduction is significantly higher than that produced in models Ia_$\delta\delta$, IIa_$\varepsilon\delta\varepsilon$, and IIa_$\varepsilon\varepsilon\varepsilon$, where Cu^{2+} and Cu^{+} atoms are interacting with neutral ligands. As a consequence, Cu^{2+}−Aβ/Cu^{+}−Aβ reaction energies are more negative for models Ia_$\delta\delta$, IIa_$\varepsilon\delta\varepsilon$, and IIa_$\varepsilon\varepsilon\varepsilon$ than for Ib_$\delta\varepsilon$ and IIc_δ, which leads to higher reduction potentials for the formers. These observations confirm that differences on the SRP for the complexes considered mainly arise from the differences in the metal environment and more, particularly, on the nature of the ligands (charged vs neutral). In addition, the comparison between the values obtained for the cluster systems and those for the Cu^{2+}−Aβ complexes highlights the importance of the changes induced by the peptide moiety.

The SRPs for all complexes are all lower than 0.30 V, and thus reduction of O_2 to H_2O_2 is thermodynamically favored for all complexes considered. Moreover, computed values indicate that the process of metal reduction could not be facilitated by any of the oxidizable amino acids present in the Aβ peptide such as Tyr10 because its redox potential is determined to be 0.95 V.[14] Thus, the participation of external reducing agents is necessary. The first step of the process, namely, the reduction of the metal center by typical external reducing agents (Figure 1), however, would not be favorable for all systems. For instance, complexes IIc_δ and IIc_ε would not be reduced by any of the typical reducing agents present in the cerebral medium implicated in the development of AD because all of them have higher SRP. Thus, they do not seem to be plausible candidates for participating in the reactions associated with the neurological damage observed in AD.[11] Complex Ib_$\delta\varepsilon$ could be reduced by agents such as NAD+ (SRP = −0.32 V)[72] and FAD (SRP = −0.33 V)[72] among others, with SRP values lower than −0.12 V. These species are typically present in the mitochondria of the neurons, taking part in the respiratory chain associated with the generation of energy.[73] Finally, complexes Ia_$\delta\delta$, IIa_$\varepsilon\delta\varepsilon$, and IIa_$\varepsilon\varepsilon\varepsilon$ can be reduced by most of the reducing species found in the cerebral medium such as ascorbic acid (SRP = 0.05 V),[74] cytochrome b (SRP = 0.04 V), myoglobin (SRP = 0.01 V), glutathione (SRP = −0.23 V), and vitamin B12 (SRP = −0.24 V)[72] among others, which are present in the extracellular medium, besides the mitochondrial species previously mentioned. Moreover, their computed SRP values are in pretty good agreement with the most recent experimental values determined for Cu^{2+}−Aβ(1−16) complex (between 0.28 and 0.34 V).[14,16,17]

IV. CONCLUSIONS

The present work determines 3D structures of various Cu^{2+}−Aβ(1−16) complexes enclosing metal coordination environments proposed from EPR experiments at different pH by combining HM techniques with QM-based approaches. In particular, we provide structures for (i) component Ia/Ib that encloses the terminal amino group, His6 and His13/His14, and an O atom from Asp1 in the coordination sphere and is dominant at pH 6 to 7, (ii) component IIa, with the three histidines (His6, His13, and His14) and the carbonyl group of Ala2 coordinating the metal cation, and (iii) component IIc with His6, the NH_2 terminus, the deprotonated amide nitrogen of Ala2, and a carbonyl oxygen interacting with Cu^{2+}, the last two proposed at pH 8 to 9. Large conformational exploration of Cu^{2+}−Aβ complexes is done with metal coordination restraints derived from QM calculations. Representative models derived from HM simulations are evaluated and finally fully refined at the DFT level (M06-2X), including solvent effects with the implicit SMD polarizable continuum model. Results show that the final stability of the complexes results from a balance between the metal coordination site and amyloid folding upon complexation, illustrating the importance of the second-coordination sphere in defining the relative stability between complexes.

SRPs of these complexes are then computed with the aim of getting new insights into the relation between their structure and their redox behavior. Results show that in all cases copper reduction induces $CO_{backbone}$ decoordination, which, for distorted square planar structures in the oxidized state (Ia_$\delta\delta$, IIa_$\varepsilon\delta\varepsilon$, IIa_$\varepsilon\varepsilon\varepsilon$, IIc_$\delta$, and IIc_$\varepsilon$), leads to tricoordinated species, in most cases, with T-shaped structure. For pentacoordinated Ib_$\delta\varepsilon$ due to the presence of the Glu11 at the apical position, reduction leads to a distorted tetrahedral structure. Moreover, results highlight the importance of the nature of the ligands on the SRP, computed values for Ib_$\delta\varepsilon$, IIc_δ, and IIc_ε (−0.12, −0.37, and −0.81), with deprotonated amide or a carboxylate in the coordination sphere, being significantly lower than those computed for models Ia_$\delta\delta$, IIa_$\varepsilon\delta\varepsilon$, and IIa_$\varepsilon\varepsilon\varepsilon$ (0.28, 0.21, and 0.19 V). These latter values are the ones in better agreement with the reported

dx.doi.org/10.1021/jp5019718 | J. Phys. Chem. B 2014, 118, 4840−4850

experimental data (~0.3 V) and are consistent with the production of H_2O_2 related to the oxidative stress characteristic of the AD.

■ ASSOCIATED CONTENT

Supporting Information

Complete refs 7, 9, 10, 18, and 60. Optimized structures for cluster systems including only the first metal coordination sphere and $Cu^{2+/+}A\beta(1-16)$ models. Reaction energies and SRP for cluster systems. Cartesian coordinates for all built $Cu^{2+/+}A\beta(1-16)$ models. This material is available free of charge via the Internet at http://pubs.acs.org.

■ AUTHOR INFORMATION

Corresponding Author

*E-mail: Mariona.Sodupe@uab.cat.

Notes

The authors declare no competing financial interest.

■ ACKNOWLEDGMENTS

We gratefully acknowledge financial support from MINECO and the Generalitat de Catalunya through CTQ2011-24847, CTQ2011-23336, and SGR2009-0638 projects, respectively, and the use of computer time at the CESCA supercomputing center. M.S. also acknowledges support through 2011 ICREA Academia award.

■ REFERENCES

(1) Alzheimer's Association, Alzheimer's Disease Facts and Figures. http://www.alz.org/downloads/facts_figures_2014.pdf (accessed 4/10/2014).

(2) Hardy, J.; Selkoe, D. J. The Amyloid Hypothesis of Alzheimer's Disease: Progress and Problems on the Road to Therapeutics. *Science* **2002**, *297* (5580), 353−356.

(3) Selkoe, D. J. Alzheimer's Disease: Genes, Proteins, and Therapy. *Physiol. Rev.* **2001**, *81* (2), 741−766.

(4) Markesbery, W. R. Oxidative Stress Hypothesis in Alzheimer's Disease. *Free Radicals Biol. Med.* **1997**, *23* (1), 134−147.

(5) Gaggelli, E.; Kozlowski, H.; Valensin, D.; Valensin, G. Copper Homeostasis and Neurodegenerative Disorders (Alzheimer's, Prion, and Parkinson's Diseases and Amyotrophic Lateral Sclerosis). *Chem. Rev.* **2006**, *106* (6), 1995−2044.

(6) Bush, A. I. The Metallobiology of Alzheimer's Disease. *Neurosciences* **2003**, *26* (4), 207−214.

(7) Nunomura, A.; Perry, G.; Aliev, G.; Hirai, K.; Takeda, A.; Balraj, E. K.; Jones, P. K.; Ghanbari, H.; Wataya, T.; Shimohama, S.; et al. Oxidative Damage is the Earliest Event in Alzheimer Disease. *J. Neuropathol. Exp. Neurol.* **2001**, *60* (8), 759−767.

(8) Mecocci, P.; Macgarvey, U.; Kaufman, A. E.; Koontz, D.; Shoffner, J. M.; Wallace, D. C.; Beal, M. F. Oxidative Damage to Mitochondrial-DNA Shows Marked Age-dependent Increases in Human Brain. *Ann. Neurol.* **1993**, *34* (4), 609−616.

(9) Huang, X. D.; Cuajungco, M. P.; Atwood, C. S.; Hartshorn, M. A.; Tyndall, J. D. A.; Hanson, G. R.; Stokes, K. C.; Leopold, M.; Multhaup, G.; Goldstein, L. E.; et al. Cu(II) Potentiation of Alzheimer A Beta Neurotoxicity - Correlation with Cell-free Hydrogen Peroxide Production and Metal Reduction. *J. Biol. Chem.* **1999**, *274* (52), 37111−37116.

(10) Opazo, C.; Huang, X.; Cherny, R. A.; Moir, R. D.; Roher, A. E.; White, A. R.; Cappai, R.; Masters, C. L.; Tanzi, R. E.; Inestrosa, N. C.; et al. Metalloenzyme-like Activity of Alzheimer's Disease Beta -amyloid. *J. Biol. Chem.* **2002**, *277* (43), 40302−40308.

(11) Barnham, K. J.; Masters, C. L.; Bush, A. I. Neurodegenerative Diseases and Oxidative Stress. *Nat. Rev. Drug Discovery* **2004**, *3* (3), 205−214.

(12) Hewitt, N.; Rauk, A. Mechanism of Hydrogen Peroxide Production by Copper-Bound Amyloid Beta Peptide: A Theoretical Study. *J. Phys. Chem. B* **2009**, *113* (4), 1202−1209.

(13) Jiang, D. L.; Li, X. J.; Williams, R.; Patel, S.; Men, L. J.; Wang, Y. S.; Zhou, F. M. Ternary Complexes of Iron, Amyloid-beta, and Nitrilotriacetic Acid: Binding Affinities, Redox Properties, and Relevance to Iron-Induced Oxidative Stress in Alzheimer's Disease. *Biochemistry* **2009**, *48* (33), 7939−7947.

(14) Jiang, D. L.; Men, L. J.; Wang, J. X.; Zhang, Y.; Chickenyen, S.; Wang, Y. S.; Zhou, F. M. Redox Reactions of Copper Complexes Formed with Different Beta-amyloid Peptides and their Neuropathalogical Relevance. *Biochemistry* **2007**, *46* (32), 9270−9282.

(15) Ali-Torres, J.; Rodriguez-Santiago, L.; Sodupe, M.; Rauk, A. Structures and Stabilities of Fe(2+/3+) Complexes Relevant to Alzheimer's Disease: An ab Initio Study. *J. Phys. Chem. A* **2011**, *115* (45), 12523−12530.

(16) Guilloreau, L.; Combalbert, S.; Sournia-Saquet, A.; Mazarguil, H.; Faller, P. Redox Chemistry of Copper-amyloid-beta: The Generation of Hydroxyl Radical in the Presence of Ascorbate is Linked to Redox-potentials and Aggregation State. *ChemBioChem.* **2007**, *8* (11), 1317−1325.

(17) Balland, V.; Hureau, C.; Saveant, J.-M. Electrochemical and Homogeneous Electron Transfers to the Alzheimer Amyloid-beta Copper Complex Follow a Preorganization Mechanism. *Proc. Natl. Acad. Sci. U.S.A.* **2010**, *107* (40), 17113−17118.

(18) Barnham, K. J.; Haeffner, F.; Ciccotosto, G. D.; Curtain, C. C.; Tew, D.; Mavros, C.; Beyreuther, K.; Carrington, D.; Masters, C. L.; Cherny, R. A.; et al. Tyrosine Gated Electron Transfer is Key to the Toxic Mechanism of Alzheimer's Disease Beta -amyloid. *FASEB J.* **2004**, *18* (12), 1427−1429.

(19) Sanaullah, G. S. W.; Glass, R. S. The Effect of pH and Complexation of Amino Acid Functionality on the Redox Chemistry of Methionine and X-ray Structure of (Co(en)-2(L-Met))(ClO-4)-2.H-20. *J. Inorg. Biochem.* **1994**, *55* (2), 87−99.

(20) Nelson, D. L.; Cox, M. M. *Lehninger Principles of Biochemistry*; W. H. Freeman: New York, 2005.

(21) Azimi, S.; Rauk, A. On the Involvement of Copper Binding to the N-terminus of the Amyloid Beta Peptide of Alzheimer's Disease: A Computational Study on Model Systems. *Int. J. Alzheimer's Dis.* **2011**, *2011*, 539762.

(22) Liu, L.; Jiang, D.; McDonald, A.; Hao, Y.; Millhauser, G. L.; Zhou, F. Copper Redox Cycling in the Prion Protein Depends Critically on Binding Mode. *J. Am. Chem. Soc.* **2011**, *133* (31), 12229−12237.

(23) Hou, L. M.; Zagorski, M. G. NMR Reveals Anomalous Copper(II) Binding to the Amyloid A Beta Peptide of Alzheimer's Disease. *J. Am. Chem. Soc.* **2006**, *128* (29), 9260−9261.

(24) Parthasarathy, S.; Long, F.; Miller, Y.; Xiao, Y.; McElheny, D.; Thurber, K.; Ma, B.; Nussinov, R.; Ishii, Y. Molecular-Level Examination of Cu2+ Binding Structure for Amyloid Fibrils of 40-Residue Alzheimer's by Solid-State NMR Spectroscopy. *J. Am. Chem. Soc.* **2011**, *133* (10), 3390−3400.

(25) Curtain, C. C.; Ali, F.; Volitakis, I.; Cherny, R. A.; Norton, R. S.; Beyreuther, K.; Barrow, C. J.; Masters, C. L.; Bush, A. I.; Barnham, K. J. Alzheimer's Disease Amyloid-beta Binds Copper and Zinc to Generate an Allosterically Ordered Membrane-penetrating Structure Containing Superoxide Dismutase-like Subunits. *J. Biol. Chem.* **2001**, *276* (23), 20466−20473.

(26) Drew, S. C.; Masters, C. L.; Barnham, K. J. Alanine-2 Carbonyl is an Oxygen Ligand in Cu2+ Coordination of Alzheimer's Disease Amyloid-β Peptide − Relevance to N-Terminally Truncated Forms. *J. Am. Chem. Soc.* **2009**, *131* (25), 8760−8761.

(27) Drew, S. C.; Noble, C. J.; Masters, C. L.; Hanson, G. R.; Barnham, K. J. Pleomorphic Copper Coordination by Alzheimer's Disease Amyloid-beta Peptide. *J. Am. Chem. Soc.* **2009**, *131* (3), 1195−1207.

(28) Guilloreau, L.; Damian, L.; Coppel, Y.; Mazarguil, H.; Winterhalter, M.; Faller, P. Structural and Thermodynamical Proper-

ties of Cu-II Amyloid-beta 16/28 Complexes Associated with Alzheimer's Disease. *J. Biol. Inorg. Chem.* **2006**, *11* (8), 1024−1038.
(29) Karr, J. W.; Akintoye, H.; Kaupp, L. J.; Szalai, V. A. N-Terminal Deletions Modify the Cu2+ Binding Site in Amyloid-beta. *Biochemistry* **2005**, *44* (14), 5478−5487.
(30) Miura, T.; Suzuki, K.; Kohata, N.; Takeuchi, H. Metal Binding Modes of Alzheimer's Amyloid beta -Peptide in Insoluble Aggregates and Soluble Complexes. *Biochemistry* **2000**, *39* (23), 7024−7031.
(31) Streltsov, V. X-ray Absorption and Diffraction Studies of the Metal Binding Sites in Amyloid Beta-peptide. *Eur. Biophys. J. Biophys. Lett.* **2008**, *37* (3), 257−263.
(32) Streltsov, V. A.; Titmuss, S. J.; Epa, V. C.; Barnham, K. J.; Masters, C. L.; Varghese, J. N. The Structure of the Amyloid-beta Peptide High-affinity Copper II Binding Site in Alzheimer Disease. *Biophys. J.* **2008**, *95* (7), 3447−3456.
(33) Syme, C. D.; Nadal, R. C.; Rigby, S. E. J.; Viles, J. H. Copper Binding to the Amyloid-beta (Abeta) Peptide Associated with Alzheimer's Disease: Folding, coordination Geometry, pH Dependence, Stoichiometry, and Affinity of Abeta -(1−28): Insights from a Range of Complementary Spectroscopic Techniques. *J. Biol. Chem.* **2004**, *279* (18), 18169−18177.
(34) Hureau, C.; Coppel, Y.; Dorlet, P.; Solari, P. L.; Sayen, S.; Guillon, E.; Sabater, L.; Faller, P. Deprotonation of the Asp1Ala2 Peptide Bond Induces Modification of the Dynamic Copper(II) Environment in the Amyloid-β Peptide near Physiological pH. *Angew. Chem., Int. Ed.* **2009**, *48* (50), 9522−9525.
(35) Dorlet, P.; Gambarelli, S.; Faller, P.; Hureau, C. Pulse EPR Spectroscopy Reveals the Coordination Sphere of Copper(II) Ions in the 1−16 Amyloid-beta Peptide: A Key Role of the First Two N-Terminus Residues. *Angew. Chem., Int. Ed.* **2009**, *48* (49), 9273−9276.
(36) Drew, S. C.; Barnham, K. J. The Heterogeneous Nature of Cu2+ Interactions with Alzheimer's Amyloid-beta Peptide. *Acc. Chem. Res.* **2011**, *44* (11), 1146−1155.
(37) Faller, P.; Hureau, C. Bioinorganic Chemistry of Copper and Zinc Ions Coordinated to Amyloid-beta Peptide. *Dalton Trans.* **2009**, No. 7, 1080−1094.
(38) Faller, P.; Hureau, C.; Berthoumieu, O. Role of Metal Ions in the Self-assembly of the Alzheimer's Amyloid-beta Peptide. *Inorg. Chem.* **2013**, *52* (21), 12193−12206.
(39) Rickard, G. A.; Gomez-Balderas, R.; Brunelle, P.; Raffa, D. F.; Rauk, A. Binding Affinities for Models of Biologically Available Potential Cu(II) Ligands Relevant to Alzheimer's Disease: An ab Initio Study. *J. Phys.Chem. A* **2005**, *109* (37), 8361−8370.
(40) Mantri, Y.; Fioroni, M.; Baik, M. H. Computational Study of the Binding of Cu-II to Alzheimer's Amyloid-beta Peptide: Do A beta 42 and A beta 40 Bind Copper in Identical Fashion? *J. Biolog. Inorg. Chem.* **2008**, *13* (8), 1197−1204.
(41) Raffa, D. F.; Rauk, A. Molecular Dynamics Study of the Beta Amyloid Peptide of Alzheimer's Disease and Its Divalent Copper Complexes. *J. Phys. Chem. B* **2007**, *111* (14), 3789−3799.
(42) Minicozzi, V.; Morante, S.; Rossi, G. C.; Stellato, F.; Christian, N.; Jansen, K. The Role of Metals in Amyloid Aggregation - Experiments and ab initio Simulations. *Int. J. Quantum Chem.* **2008**, *108* (11), 1992−2015.
(43) Marino, T.; Russo, N.; Toscano, M.; Pavelka, M. On the Metal Ion (Zn2+, Cu2+) Coordination with beta-amyloid Peptide: DFT Computational Study. *Interdiscip. Sci.: Comput. Life Sci.* **2010**, *2*, 57−69.
(44) Alí-Torres, J.; Maréchal, J.-D.; Rodríguez-Santiago, L.; Sodupe, M. Three Dimensional Models of Cu2+-Aβ(1−16) Complexes from Computational Approaches. *J. Am. Chem. Soc.* **2011**, *133* (38), 15008−15014.
(45) Furlan, S.; Hureau, C.; Faller, P.; La Penna, G. Modeling Copper Binding to the Amyloid-beta Peptide at Different pH: Toward a Molecular Mechanism for Cu Reduction. *J. Phys.Chem. B* **2012**, *116* (39), 11899−11910.
(46) La Penna, G.; Hureau, C.; Andreussi, O.; Faller, P. Identifying, By First-Principles Simulations, Cu Amyloid-beta Species Making Fenton-Type Reactions in Alzheimer's Disease. *J. Phys. Chem. B* **2013**, *117* (51), 16455−16467.
(47) Zirah, S.; Kozin, S. A.; Mazur, A. K.; Blond, A.; Cheminant, M.; Segalas-Milazzo, I.; Debey, P.; Rebuffat, S. Structural Changes of Region 1−16 of the Alzheimer Disease Amyloid beta -Peptide upon Zinc Binding and in Vitro Aging. *J. Biol. Chem.* **2006**, *281* (4), 2151−2161.
(48) Šali, A.; Webb, B.; Madhusudhan, M. S.; Shen, M.-Y.; Marti-Renom, M. A.; Eswar, N.; Alber, F.; Topf, M.; Oliva, B.; Fiser, A.; Sánchez, R.; Yerkovich, B.; Badretdinov, A.; Melo, F.; Overington, J. P.; Feyfant, E. *MODELLER A Program for Protein Structure Modeling 9v5*, 2007
(49) Pettersen, E. F.; Goddard, T. D.; Huang, C. C.; Couch, G. S.; Greenblatt, D. M.; Meng, E. C.; Ferrin, T. E. UCSF Chimera - A Visualization System for Exploratory Research and Analysis. *J. Comput. Chem.* **2004**, *25* (13), 1605−1612.
(50) Colovos, C.; Yeates, T. O. Verification of Protein Structures - Patterns of Nonbonded Atomic Interactions. *Protein Sci.* **1993**, *2* (9), 1511−1519.
(51) Rios-Font, R.; Sodupe, M.; Rodriguez-Santiago, L.; Taylor, P. R. The Role of Exact Exchange in the Description of Cu2+-(H2O)(n) (n=1−6) Complexes by Means of DFT Methods. *J. Phys. Chem. A* **2010**, *114* (40), 10857−10863.
(52) Georgieva, I.; Trendafilova, N.; Rodriguez-Santiago, L.; Sodupe, M. Coordination Properties of the Oxime Analogue of Glycine to Cu(II). *J. Phys. Chem. A* **2005**, *109* (25), 5668−5676.
(53) Zhao, Y.; Truhlar, D. G. The M06 Suite of Density Functionals for Main Group Thermochemistry, Thermochemical Kinetics, Noncovalent Interactions, Excited States, and Transition Elements: Two New Functionals and Systematic Testing of Four M06-class Functionals and 12 Other Functionals. *Theor. Chem. Acc.* **2008**, *120* (1−3), 215−241.
(54) National Institute of Standards and Technology. http://physics.nist.gov/PhysRefData/Handbook/Tables/coppertable1.htm (accessed 04/10/2014).
(55) Hay, P. J.; Wadt, W. R. Ab Initio Effective Core Potentials for Molecular Calculations. Potentials for K to Au Including the Outermost Core Orbitals. *J. Chem. Phys.* **1985**, *82* (1), 299−310.
(56) Roy, L. E.; Hay, P. J.; Martin, R. L. Revised Basis Sets for the LANL Effective Core Potentials. *J. Chem. Theory Comput.* **2008**, *4* (7), 1029−1031.
(57) Ehlers, A. W.; Bohme, M.; Dapprich, S.; Gobbi, A.; Hollwarth, A.; Jonas, V.; Kohler, K. F.; Stegmann, R.; Veldkamp, A.; Frenking, G. A Set of f Polarization Functions for Pseudo-potential Basis Sets of the Transition Metals Sc-Cu, Y-Ag and La-Au. *Chem. Phys. Lett.* **1993**, *208* (1−2), 111−114.
(58) Marenich, A. V.; Cramer, C. J.; Truhlar, D. G. Universal Solvation Model Based on Solute Electron Density and on a Continuum Model of the Solvent Defined by the Bulk Dielectric Constant and Atomic Surface Tensions. *J. Phys. Chem. B* **2009**, *113* (18), 6378−6396.
(59) Ali-Torres, J.; Dannenberg, J. J. The Folding of Acetyl(Ala)(28)NH2 and Acetyl(Ala)(40)NH2 Extended Strand Peptides into Antiparallel beta-Sheets. A Density Functional Theory Study of beta-Sheets with beta-Turns. *J. Phys. Chem. B* **2012**, *116* (48), 14017−14022.
(60) Frisch, M. J.; Trucks, G. W.; Schlegel, H. B.; Scuseria, G. E.; Robb, M. A.; Cheeseman, J. R.; Scalmani, G.; Barone, V.; Mennucci, B.; Petersson, G. A. et al. *Gaussian 09*, revision A.02; Gaussian, Inc.: Wallingford, CT, 2009.
(61) Wagman, D. D.; E, W. H.; Parker, V. B.; Schumm, R. H.; Halow, I.; Bailey, S. M.; Churney, K. L.; Nuttall, R. L. The NBS Tables of Chemical Thermodynamic Properties. Selected values for Inorganic and C-1 and C-2 organic substances in SI units. *J. Phys. Chem.* **1982**, *Ref Data Supl 1*, 11.
(62) El Khoury, Y.; Dorlet, P.; Faller, P.; Hellwig, P. New Insights into the Coordination of Cu(II) by the Amyloid-B 16 Peptide from Fourier Transform IR Spectroscopy and Isotopic Labeling. *J. Phys. Chem. B* **2011**, *115* (49), 14812−14821.

(63) Bard, A. J.; Parsons, R.; Jordan, J. *Standard Potentials in Aqueous Solutions*; Marcel Dekker: New York, 1985.
(64) Himes, R. A.; Park, G. Y.; Barry, A. N.; Blackburn, N. J.; Karlin, K. D. Synthesis and X-ray Absorption Spectroscopy Structural Studies of Cu(I) Complexes of HistidylHistidine Peptides: The Predominance of Linear 2-Coordinate Geometry. *J. Am. Chem. Soc.* **2007**, *129* (17), 5352−5353.
(65) Himes, R. A.; Park, G. Y.; Siluvai, G. S.; Blackburn, N. J.; Karlin, K. D. Structural Studies of Copper(I) Complexes of Amyloid-beta Peptide Fragments: Formation of Two-Coordinate Bis(histidine) Complexes. *Angew. Chem., Int. Ed.* **2008**, *47* (47), 9084−9087.
(66) Shearer, J.; Szalai, V. A. The Amyloid-beta Peptide of Alzheimer's Disease Binds Cu(I) in a Linear Bis-His Coordination Environment: Insight into a Possible Neuroprotective Mechanism for the Amyloid-beta Peptide. *J. Am. Chem. Soc.* **2008**, *130* (52), 17826−17835.
(67) Raffa, D. F.; Rickard, G. A.; Rauk, A. Ab Initio Modelling of the Structure and Redox Behaviour of Copper(I) Bound to a His-His Model Peptide: Relevance to the beta-Amyloid Peptide of Alzheimer's Disease. *J. Biol. Inorg. Chem.* **2007**, *12* (2), 147−164.
(68) Rimola, A.; Constantino, E.; Rodriguez-Santiago, L.; Sodupe, M. Binding Properties of Cu+/2+-(glycyl)nglycine Complexes (n = 1−3). *J. Phys. Chem. A* **2008**, *112* (15), 3444−3453.
(69) Furlan, S.; Hureau, C.; Faller, P.; La Penna, G. Modeling the Cu(+) Binding in the 1−16 Region of the Amyloid-beta Peptide Involved in Alzheimer's Disease. *J. Phys. Chem. B* **2010**, *114* (46), 15119−15133.
(70) Cassagnes, L.-E.; Herve, V.; Nepveu, F.; Hureau, C.; Faller, P.; Collin, F. The Catalytically Active Copper-amyloid-Beta State: Coordination Site Responsible for Reactive Oxygen Species Production. *Angew. Chem., Int. Ed.* **2013**, *52* (42), 11110−11113.
(71) Peck, K. L.; Clewett, H. S.; Schmitt, J. C.; Shearer, J. Copper Ligation to Soluble Oligomers of the English Mutant of the Amyloid-beta Peptide Yields a Linear Cu(I) Site that Is Resistant to O-2 Oxidation. *Chem. Commun.* **2013**, *49* (42), 4797−4799.
(72) Dryhurst, G.; Kadish, K. M.; Scheller, F.; Renneberg, R. *Biol. Electrochem.*; Academic Press: New York, 1982; Vol. *1*.
(73) Wallace, D. C. Diseases of the Mitochondrial-DNA. *Annu. Rev. Biochem.* **1992**, *61*, 1175−1212.
(74) Conway, B. E. *Electrochemical Data*; Greenwood Press: Westport, CT, 1969.